Trends and Transitions in Silicate Weathering in the Asian Interior (NE Tibet) Since 53 Ma

Yibo Yang, Wenxia Han, Chengcheng Ye, Albert Galy, Xiaomin Fang

frontiers in Earth Science

ORIGINAL RESEARCH
published: 23 February 2022
doi: 10.3389/feart.2022.824404

Trends and Transitions in Silicate Weathering in the Asian Interior (NE Tibet) Since 53 Ma

Yibo Yang[1], Wenxia Han[2]*, Chengcheng Ye[3], Albert Galy[4] and Xiaomin Fang[1,5]*

[1]State Key Laboratory of Tibetan Plateau Earth System Science, Resources and Environment (TPESRE), Institute of Tibetan Plateau Research, Chinese Academy of Sciences, Beijing, China, [2]Shandong Provincial Key Laboratory of Water and Soil Conservation and Environmental Protection, College of Resources and Environment Sciences, Linyi University, Linyi, China, [3]School of Environmental and Geographical Science, Shanghai Normal University, Shanghai, China, [4]Centre de Recherches Pétrographiques et Géochimiques, UMR7358, CNRS - Université de Lorraine, Vandoeuvre Les Nancy, France, [5]University of Chinese Academy of Sciences, Beijing, China

The relationship between silicate weathering, Tibetan Plateau uplift, and global cooling during the Cenozoic provides a valuable case study for understanding the interaction of tectonics and climate. The Tibetan Plateau uplift is considered to have caused Cenozoic cooling via the atmospheric CO_2 drawdown by increased silicate weathering. However, this hypothesis has been intensively debated over the past few decades due to the lack of complete silicate weathering records from the continental interior, which can directly track the effects of uplift on weathering. We provide the first complete long (past 53 Myr) continental silicate weathering record from the NE Tibetan Plateau, combined with a comprehensive analysis on its evolution pattern, critical transitions, and associated driving forces. The silicate weathering intensity in NE Tibet is characterized by a long-term Paleogene decrease, modulated by global cooling, and a Neogene increase that may be related to the East Asian summer monsoon (EASM) intensification. Three major system transitions in regional silicate weathering are identified at ~26–23 Ma, ~16 Ma and ~8 Ma, which are linked to enhanced EASM forced primarily by tectonic uplift at these intervals, with some surbordinate influences from global climate at ~16 Ma. We also capture an intensification of the 100-kyr cycle at ~16 Ma and ~8 Ma in the obtained silicate weathering record, which is in coincidence in time with the enhancement of the EASM. This might suggest some contribution of the Antarctic ice sheets on modulating the regional silicate weathering in the NE Tibetan Plateau on a timescale of 10^5–10^6 years, through its influences on the EASM as proposed by previous studies.

Keywords: Cenozoic, chemical weathering, tectonic uplift, global cooling, Asian monsoon, clay mineral, Antarctic ice sheets, eccentricity cycle

OPEN ACCESS

Edited by:
Steven L. Forman,
Baylor University, United States

Reviewed by:
Rui Zhang,
Northwest University, China
Xiaoqiang Yang,
Sun Yat-sen University, China

****Correspondence:***
Yibo Yang
yangyibo@itpcas.ac.cn
Wenxia Han
wenxia_han@163.com

Specialty section:
This article was submitted to Quaternary Science, Geomorphology and Paleoenvironment, a section of the journal Frontiers in Earth Science

Received: *29 November 2021*
Accepted: *31 January 2022*
Published: *23 February 2022*

Citation:
Yang Y, Han W, Ye C, Galy A and Fang X (2022) Trends and Transitions in Silicate Weathering in the Asian Interior (NE Tibet) Since 53 Ma. Front. Earth Sci. 10:824404. doi: 10.3389/feart.2022.824404

INTRODUCTION

Continental silicate weathering plays a critical role in stabilizing Earth's climate system and habitability in the long term (Walker et al., 1981). Cenozoic uplift of the Himalaya-Tibetan Plateau was suggested to have caused global cooling via the weathering of fresh silicate minerals (Raymo and Ruddiman, 1992). Over the past few decades, numerous studies have attempted to validate the evidence chain of the uplift-weathering hypothesis in diverse ways (e.g., Richter

et al., 1992; Kump and Arthur, 1997; Blum et al., 1998; Misra and Froelich, 2012; Maher and Chamberlain, 2014; Lenard et al., 2020), in the course of which several new hypotheses have been proposed (e.g., France-Lanord and Derry, 1997; Caves Rugenstein et al., 2019; Guo et al., 2021). Long-term seawater Sr, Li, Os, Mg, and Be isotope records (Peucker-Ehrenbrink et al., 1995; McCauley and Depaolo, 1997; Willenbring and Von Blanckenburg, 2010; Misra and Froelich, 2012; Higgins and Schrag, 2015; Paytan et al., 2021) provide constraints on the delivery of continentally-derived elements to the ocean, which is related to global continental silicate weathering. However, due to the lack of complete Cenozoic silicate weathering records from the Himalaya-Tibetan Plateau, the role of tectonic forcing of the global climate system remains unclear.

The thick and continuous sequence of fluvial-lacustrine sediments in the NE Tibetan Plateau that have accumulated since the early Eocene is a rich source of information on the history of plateau uplift and climate change in the Asian interior (Fang et al., 2019a). This sedimentary archive can provide a continuous record of the response of silicate weathering to the weak uplift of the NE Tibetan Plateau during the Paleogene and rapid uplift during the Neogene (Tapponnier et al., 2001; Yang et al., 2021a). During the past decade, multiple long-term records of silicate weathering history have been acquired from the NE Tibetan Plateau and the adjacent Chinse Loess Plateau, based on element ratios (Song et al., 2013; Sayem et al., 2018; Bao et al., 2019; Ren et al., 2020) and clay minerals (Zhang and Guo, 2014; Sun et al., 2015; Zhang C. et al., 2015; Fang et al., 2016a; Song B. et al., 2018; Song Y. et al., 2018; Ye et al., 2018; Fang et al., 2019b; Liu et al., 2019; Yang et al., 2019; Liu et al., 2020; Ye et al., 2020; Yang et al., 2021b; Zhao et al., 2021). However, the available silicate weathering records from the region are fragmentary because they are derived from diverse time intervals from multiple sections/basins, and they lack comparability due to the use of different elements and minerals. Therefore, a long and continuous weathering record based on a consistent methodology is needed to elucidate the temporal evolution of regional silicate weathering and the controlling mechanisms.

Silicate weathering in the upper continental crust involves the removal of base cations such as Ca, Na, K, and Mg and the concomitant formation of clay minerals (Nesbitt and Young, 1982). There is a substantial sorting effect on element abundances in sediments (Guo et al., 2018), although its impact on the relative contents of clay minerals in the clay fraction of sediments can be largely eliminated. Here, we present the first continuous record of long-term Cenozoic silicate weathering intensity (SWI) history from the NE Tibetan Plateau, based on a compilation of clay mineral data from previously published records, supplemented by new data acquired in this study. The observed decrease in SWI in the Paleogene and increase in the Neogene were modulated by a cooling global climate and by a rise in regional monsoon rainfall, respectively. Additionally, three major transitions, at ~26–23 Ma, ~16 Ma, and ~8 Ma, represent enhancements of the East Asian summer monsoon (EASM) together with an intensified 100-kyr eccentricity cycle.

MATERIALS AND METHODS

The NE Tibetan Plateau consists of complexly deformed terranes. Crystalline basement in the NE Tibetan Plateau is composed of the Qilian Shan and East Kunlun-Qaidam terranes (**Figure 1B**), which are Proterozoic and Paleozoic assemblages accreted to the Tarim and Sino-Korean cratons during Paleozoic-early Mesozoic closure of the Tethys Ocean (Yin and Harrison, 2000; Bush et al., 2016). To the north-northeast, the Qilian Shan located along the northeastern margin of the Tibetan Plateau (**Figure 1B**), has provided the primary source area for late Cenozoic fluvial-lacustrine rocks in adjacent drainage basins and eolian sequences in the downwind region, e.g., the Chinese Loess Plateau (Chen and Li, 2013; Pullen et al., 2021). The Qilian Shan has experienced multiple episodes of tectonic deformation, including Neoproterozoic continental breakup, early Paleozoic subduction and continental collision, Mesozoic extension, and Cenozoic intracontinental orogenesis resulting from the India-Asia collision (Zuza et al., 2018). To the south, the northern part of the Eastern Kunlun-Qaidam terrane is mostly occupied by the Qaidam basin. The south part of the Eastern Kunlun-Qaidam terrane is dominated by a broad Early Paleozoic arc, on which a younger and narrower Late Permian to Triassic arc was superposed (Yin and Harrison, 2000). The East Kunlun Shan was assumed to provide an important source area for early Cenozoic fluvial-lacustrine sediments in adjacent drainage basins resulting from the India-Asia collision (Clark et al., 2010; Wang et al., 2017; Yang et al., 2021a).

Given the complex geological setting in such a broad region of the NE Tibetan Plateau, comparability between clay mineral records based on semiquantitative identification methods is needed to be considered firstly for a synthesis of clay mineral records from diverse locations and time intervals. Therefore, we used clay mineral data derived using the same sample pre-treatment procedure (to obtain the clay component) and a consistent semiquantitative identification method based on X-ray diffraction (**Supplementary Figure S1**) to provide the necessary methodological consistency. The pre-treatment and identification methods were clearly stated in Fang et al. (2019b). In our compilation, including previous and new data, illite/smectite (I/S) mixed-layer clays and the percentage of smectite layers in it were identified, because both of them are useful indicators of diagenetic impact in old sedimentary sequences (e.g., Weaver, 1984).

A clay mineral assemblage, the smectite/(illite + chlorite) ratio, was used as an indicator of SWI because of its demonstrated effectiveness as a weathering index in North China in modern and Cenozoic contexts (Fang et al., 2019b; Yang et al., 2021b). In the Cenozoic sections of the region, clay minerals are mainly composed of abundant I/S mixed-layer clays and illite, with minor smectite, kaolinite, and chlorite (**Supplementary Figure S1**). I/S mixed-layer clays with varying proportions of smectites layers in different sections (**Supplementary Datasets S1-S3**) are mostly transitional products of smectite alteration during burial or illite weathering products in catchment weathering (Chamley, 1989; Weaver, 1989). Here, we did not try to distinguish the formation mechanism of the I/S mixed-layer clays because both

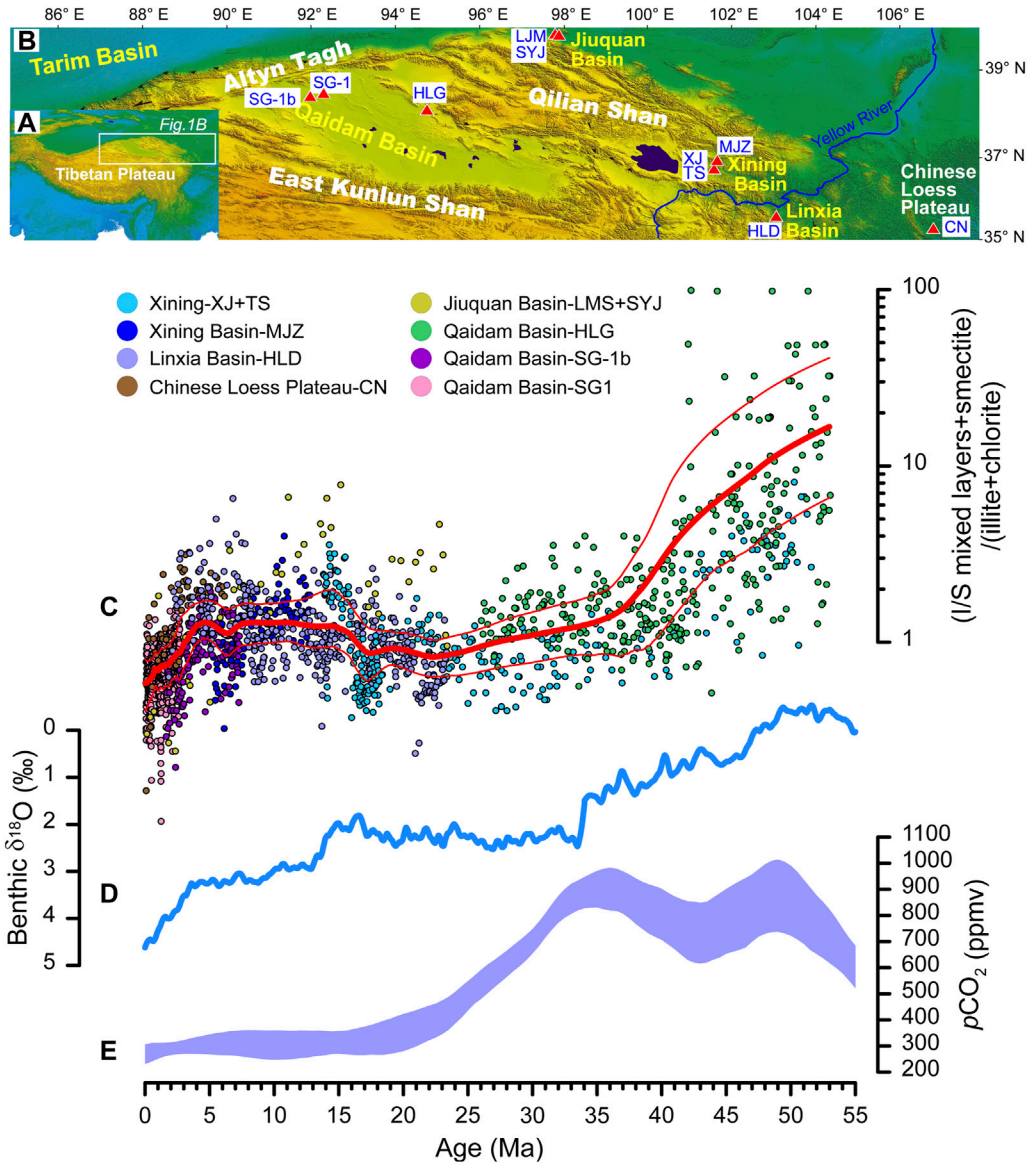

FIGURE 1 | Cenozoic silicate weathering history in the NE Tibetan Plateau **(A-B)** Map of the NE Tibetan Plateau showing site locations **(C)** Compiled (I/S mixed layer + smectite)/(illite + chlorite) ratio from the ten studied sections. The red lines show the results of locally-weighted scatterplot smoothing (LOWESS, smoothing factor 0.1) and the corresponding uncertainty envelope **(D)** Benthic oxygen isotope record (Westerhold et al., 2020) **(E)** Proxy-based atmospheric CO_2 content (Foster et al., 2017).

formation mechanisms point to an enhanced chemical weathering intensity in a relatively temperate-humid setting (Chamley, 1989), which is in contrast to the dominant occurrences of illite and chlorite in an arid and cold setting with a weakened chemical weathering intensity. We here used the (I/S mixed layer + smectite)/(illite + chlorite) ratio to represent paleo-weathering conditions. The total content of I/S mixed-layer clays, smectite, illite and chlorite comprises up to ~90% of the clay fraction (the remanent is minor kaolinite). Thus, we regard the (I/S mixed layer + smectite)/(illite + chlorite) proxy as the best candidate for tracing SWI at a regional scale.

The integrated dataset is based on sedimentary sequences from the sedimentary basins in NE Tibet: the Qaidam Basin (HLG section, 53–26 Ma, Fang et al., 2019b; core SG-1b, 7.3–1.6 Ma, Fang et al., 2016a; core SG-1, 2.8–0.1 Ma, Li M. et al., 2018), Xining Basin (XJ section, 51.5–26 Ma, Fang et al., 2019b; MJZ section, 12.8–5.3 Ma, Yang et al., 2019), Linxia Basin (upper HLD section, 12.2–1.8 Ma, Yang et al., 2021b), Jiuquan Basin (LMS and SYJ sections, 23.4–0.1 Ma, Liu et al., 2020), and the eastern Chinese Loess Plateau (CN eolian section, 6.2–0.1 Ma, Yang et al., 2021b). The clay data from the ten sections were collected in various sediment facies, such as fluvial-lacustrine facies and eolian deposits. The distinct sedimentary facies with different coarse-fine lithologies indicates a varying degree of sorting during transport. However, because our clay data are all from clay-sized fractions of samples, and we use the clay

mineral ratio (I/S mixed layer + smectite)/(illite + chlorite) rather than clay content to represent paleo-weathering conditions, the sorting effect on the proxy reliability could be greatly eliminated.

To address the problem of a low temporal resolution between 26 Ma and ~13 Ma (only 19 data values from the Jiuquan Bain), we obtained 387 new clay mineral data in this study (**Supplementary Datasets S1-S3**), including from the HZ core corresponding to the lower HLD section (228 samples, 23.3–12.3 Ma, Fang et al., 2016b) in the Linxia Basin, the upper XJ section (67 samples, 26–16.5 Ma; Dai et al., 2006) and the TS core at the top of the XJ section (92 samples, 18.4–13.8 Ma; Zan et al., 2015) from the Xining Basin. A total of 1,861 clay mineral data were obtained from these tine sections (see **Figure 1** for site locations), based on precise magnetostratigraphic age control spanning the interval from 53 Ma to the present (**Supplementary Dataset S4**), with a mean temporal resolution of ~28 kyr.

In order to show the long-term trend of the clay data, we used the locally weighted polynomial regression (LOESS, Cleveland and Devin, 1988) of the (I/S mixed layer + smectite)/(illite + chlorite) series with a smooth factor of 0.1. For a clay data point, a subset of the data around the data can be used with more weight to points near the data point and less weight to points further away. The smooth factor is the fraction of the total number of data points that are used in each local fit. A smooth factor of 0.1 is thus suitable to produce a curve that describes the deterministic part of the variation in the clay data on a scale of several million years.

In order to detect possible nonlinear dynamical transitions in the SWI record, and to facilitate an evaluation of the underlying regulating driving mechanism(s), we performed recurrence analysis. Recurrence analysis provides independent information about nonlinear dynamics, dynamical transitions, and even nonlinear interrelationships (Marwan et al., 2007). In a recurrence analysis plot, the recurrence analysis results identify the extent to which the silicate weathering system can 'repeat' itself, in which periodic processes are evident as a dark-shaded area on the plot (longer lines and less single or isolated recurrence points), whilst chaotic/stochastic fluctuations (less predictable) are evident as an unshaded area (very short lines or isolated recurrence points), and the transition between different states captures important regime changes.

RESULTS

The synthesized SWI curve for the NE Tibetan Plateau displays several noteworthy features. First, the clay mineral records from the ten sections spanning a broad region (92°-107°E, 35°-40°N) can be readily overlapped and show consistent trends (**Figure 1C**). These observations confirm the validity of using the records to produce a synthesis SWI for the region. The Jiuquan Basin data for ~10–23 Ma have much higher (I/S mixed layer + smectite)/(illite + chlorite) ratios than the records from the Xining and Linxia Basins, but the low-resolution Jiuquan Basin data do not affect the general long-term trend of the SWI, as shown by a LOESS fitted data (**Supplementary Figure S2**). This suggests that the long-term SWI trend is little influenced by several extreme values. Second, the SWI for the Paleogene shows a long-term decrease, which is similar to the long-term Paleogene global cooling trend (**Figure 1D**), within the context of relatively high atmospheric CO_2 concentrations (**Figure 1E**). Third, the SWI for the Neogene is substantially increased and shows a different evolutionary pattern from that of the global climate, within the context of generally low atmospheric CO_2 levels (**Figure 1**). The SWI rises gradually from ~23 Ma, and there is a subsequent rapid and moderate rise after ~16 Ma, followed by a distinct decrease at ~4–3 Ma.

DISCUSSION

Reliability of Clay Mineral Assemblages as a Silicate Weathering Indicator

Authigenic and diagenetic clays can bias the weathering significance of clay mineral assemblages. Previous studies have demonstrated that authigenic clay mineral formation is rare in riverine and lake systems (e.g., Fang et al., 2019b; Yang et al., 2019). Although we assume that the I/S mixed-layer clays are partially a diagenetic product of smectite, the impact of diagenesis on the (I/S mixed layer + smectite)/(illite + chlorite) ratio is insignificant. Burial diagenesis can lead to a transformation of smectite to illite with the rise in temperature and pressure caused by the rise of the burial depth. A classical diagenetic trend is the occurrence of a high proportion of illite in I/S mixed-layers and an increasing illite content with depth (Weaver, 1984), resulting in a low (I/S mixed layer + smectite)/(illite + chlorite) ratio in older samples. However, this pattern is contrary to the SWI curve, which shows high (I/S mixed layer + smectite)/(illite + chlorite) ratios in the older samples. Therefore, we consider that the clay minerals in our records are dominated by the erosion and the weathering of bedrock, not by diagenesis.

The input of recycled clays with rapid exhumation could also result in a misinterpretation of the weathering significance of clay mineral assemblages. In contrast to smectite, illite and chlorite are common constituents of older sediments due to their stability during burial (Chamley, 1989). They are also the physical product of magmatic or metamorphic rocks because physical weathering can result in mica exfoliation, feldspar sericitization and silicate chloritization in such rocks (Chamley, 1989). Recycled illite and chlorite following uplift and exhumation should thereby be considered. Our clay mineral data are from the ten sections in diverse local settings. Both the recycled clay input and the potential impact of rapid tectonics-driven erosion in each section could be related to the sedimentation rate change in each section. Plots of the sedimentation rates of the ten sections were estimated from their age-depth (thickness) relationship (**Figure 2B**). The sedimentation rates vary from <10 to 500 m/Ma, and there are distinct patterns of variation between sections, which may be caused by local depositional histories. The variable and complex pattern of sedimentation rates among the sections contrasts with the

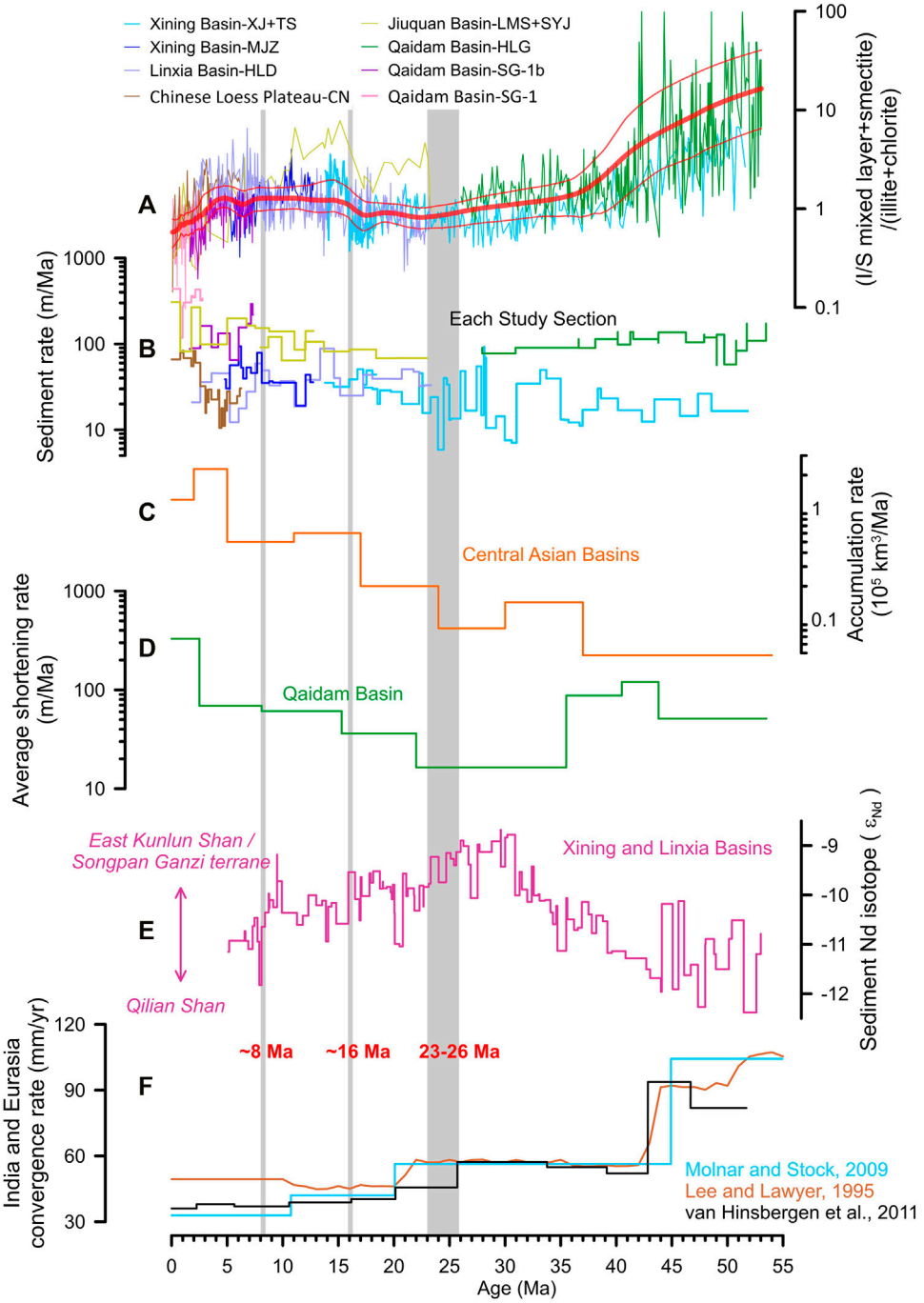

FIGURE 2 | Cenozoic silicate weathering history in the NE Tibetan Plateau and its comparison with proveannce, erosion and tectonic records **(A)** Compiled (I/S mixed layer + smectite)/(illite + chlorite) ratio **(B)** Sedimentation rates of the study sections (Xining Basin: XJ section, Dai et al., 2006; TS core, Zan et al., 2015; MJZ section, Yang et al., 2017; Qaidam Basin: SG-1 core, Zhang et al., 2012; SG-1b core, Zhang et al., 2014; HLG section, Fang et al., 2019b; Linxia Basin: HLD section and HZ core, Fang et al., 2016; Jiuquan Basin: LJM section, Fang et al., 2005; SYJ section, Song, 2006; Chinese Loess Plateau: CN section, Song et al., 2001) **(C)** Average accumulation rate in Central Asian basins (Métivier et al., 1999) **(D)** Average shortening rate in the Qaidam Basin (Bao et al., 2017) **(E)** Nd isotope of decarbonated bulk sediments from the Xining and Linxia Basins (He et al., 2019; Yang et al., 2021a) **(F)** Convergence rates between India and Eurasia (Lee and Lawver, 1995; Molnar and Stock, 2009; van Hinsbergen et al., 2011).

generally consistent trends of the (I/S mixed layer + smectite)/(illite + chlorite) ratios, suggesting a limited impact of local/regional erosion and recycled inputs on the SWI curve.

Furthermore, an intense erosion is expected to result in a lower degree of weathering and thus the formation of illite- and chlorite-rich weak alteration products of silicate minerals (e.g.,

Yang et al., 2021b; Song et al., 2021). The gradual increase in basin sedimentation flux of basin in Central Asia (**Figure 2C**, Métivier et al., 1999) and in the Qaidam Basin (**Figure 2D**, Bao et al., 2017) since the late Oligocene-early Miocene thus implies an enhanced regional erosion. The inferred strong erosion is opposite to the increase in (I/S mixed layer + smectite)/(illite + chlorite) ratio since then, thus precluded a major impact of rapid erosion on the silicate weathering intensity.

Provenance is an essential factor that could influence clay mineral assemblages. Despite the complex tectonic evolution of the NE Tibetan Plateau, the Eocene red mudstone intercalated with layers of gypsum, which was assumed to be aeolian dust, showed an identical provenance with the Quaternary loess (Licht et al., 2016). Because the NE Tibetan Plateau was the primary source for such eolian materials during the Paleogene and Neogene (Chen and Li, 2013; Nie et al., 2015; Licht et al., 2016; Pullen et al., 2021), the stable aeolian provenance probably suggests a relatively stable provenance for fine-grained detritus from the NE Tibetan Plateau (**Figure 2E**; Yang et al., 2021a). Sediment Nd isotope is useful to indicate a change in provenance linked to the mean age of the provenance and its crust/mantle affinity (e.g., McLennan et al., 1993). The ε_{Nd} (0) values in the Xining Basin and Linxia Basins range from −8.5 to 12.5 (**Figure 2E**), which are close to the typical felsic upper continental crust (e.g., McLennan et al., 1993). Nd isotope variations were thought to have been caused by the northward growth of the northern Tibetan Plateau; that is, the uplift and exhumation of the East Kunlun Shan/Songpan-Ganzi terrane since ~42 Ma, and the enhanced exhumation of the Qilian Shan ~25 Ma (Yang et al., 2021a). Such changes in sediment provenance in the NE Tibetan Plateau are generally consistent with the decrease in the convergence rate between India and Eurasia (**Figure 2F**), thus suggesting a two-stage northward growth of the northern Tibetan Plateau (Yang et al., 2021a). However, the provenance change cannot explain the variations in the SWI, for the following reasons. First, at a regional scale, the main parent minerals of newly-formed clays (e.g., feldspars and micas) are widespread in various lithologies of the upper continental crust. Second, a detailed study of the MJZ section in the Xining Basin demonstrated that the (I/S mixed layer + smectite)/(illite + chlorite) ratio is relatively uninfluenced by the provenance (Yang et al., 2019).

Besides, remote aeolian input could also result in provenance change because we cannot exclude the potential remote dust input from the Central Asian Orogenic Belt into the NE Tibetan Plateau during the late Cenozoic Asian dust expansion periods. The Central Asian Orogenic Belt is composed of young dominantly mantle-derived volcanic and plutonic rocks, showing a distinct provenance regime with less negative ε_{Nd} (0) values compared with the North Tibetan Plateau (Yang et al., 2021a). Clay-sized mineral and elemental records in the Jiuquan Basin in the northern Qilian Shan indicate that a large amount of aeolian dust input from the Tianshan-Altay Orogens into the Jiuquan Basin at ~9–8 Ma (Yang et al., 2021c). However, such remote aeolian input may less alter our main conclusion. First, the great expansion of Asian dust from Tianshan-Altay Orogens was initiated in the late Miocene. Second, the high contents of illite and chlorite input from arid central Asia are consistent with the general drying with weakened silicate weathering in the northern Tibetan Plateau (Liu et al., 2020).

Regional Weathering History and Major Transitions

After excluding the potential impacts of authigenic, diagenetic and recycled clays, and rapid erosion and provenance effects, we interpret the long-term evolutionary trends of the SWI records to be caused mainly by climatic factors. Global climate change is the first such factor to be addressed. Cooling is assumed to be the dominant factor regulating the variation of the SWI in NE Tibet during the Paleogene (Fang et al., 2019b). The regulatory mechanisms include the direct impact of temperature on silicate weathering reactions by the Arrhenius law and the supply of moisture from the Paratethys Sea by the Westerlies, modulated by the global temperature regime (Fang et al., 2019b). The significant negative correlation between the (I/S mixed layer + smectite)/(illite + chlorite) ratio and the benthic $\delta^{18}O$ record (Westerhold et al., 2020) during the interval of 53 to ~26–23 Ma (53–26 Ma, r = −0.88, $p < 0.0001$, **Figure 3A**) supports the dominant control of Paleogene cooling on long-term regional weathering and climate in the NE Tibetan Plateau. This is also supported by other studies showing that Paleogene cooling modulated regional aridity within the NE Tibetan Plateau (Li J. X. et al., 2018; Sun et al., 2020). Additionally, after ~4–3 Ma the (I/S mixed layer + smectite)/(illite + chlorite) ratio and the benthic $\delta^{18}O$ record are also negatively correlated (r = −0.97, $p < 0.0001$), similar to the relationship before ~26–23 Ma (**Figure 3A**), which also indicates the predominant control of global cooling on Northern Hemisphere climate, in an Icehouse, on regional weathering in the NE Tibetan Plateau.

However, the correlation between the (I/S mixed layer + smectite)/(illite + chlorite) ratio and the benthic $\delta^{18}O$ record (Westerhold et al., 2020) after ~26–23 Ma is inconsistent, showing a 'looped' pattern until ~4–3 Ma with an overall positive correlation (26–3.3 Ma, r = 0.68, $p < 0.0001$), which differs from the previous roughly negative relationship (**Figure 3A**). This 'looped' pattern implies an emerging driving factor that was different from the global climate state that regulated the regional SWI after ~26–23 Ma. To further analyze the changes in the relationship between the SWI and the global $\delta^{18}O$ record, we performed the recurrence analysis. The recurrence plot of (I/S mixed layer + smectite)/(illite + chlorite) ratio reveals three distinct system transitions within the SWI record: at ~26–23 Ma, ~16 Ma and ~8 Ma (**Figure 3B**, indicated by red arrows). At each section, the three transitions mark the onset of an enhanced SWI: for example, in the Jiuquan, Xining and Linxia Basins at ~23–21 Ma and ~16 Ma, and in the Linxia Basin at ~8 Ma (**Figure 2A**). It should be noted that ~8 Ma corresponds to the onset of an enhanced SWI in the Linxia Basin (Yang et al., 2021b) and the Chinese Loess Plateau (Sun et al., 2015); while due to mountain uplift in NE Tibet, the rain-shadow effect led to a weakened SWI in the Xining and Jiuquan Basins (see the detailed discussion in Yang et al., 2021b). Therefore, the averaged SWI curve remains stable at ~8 Ma.

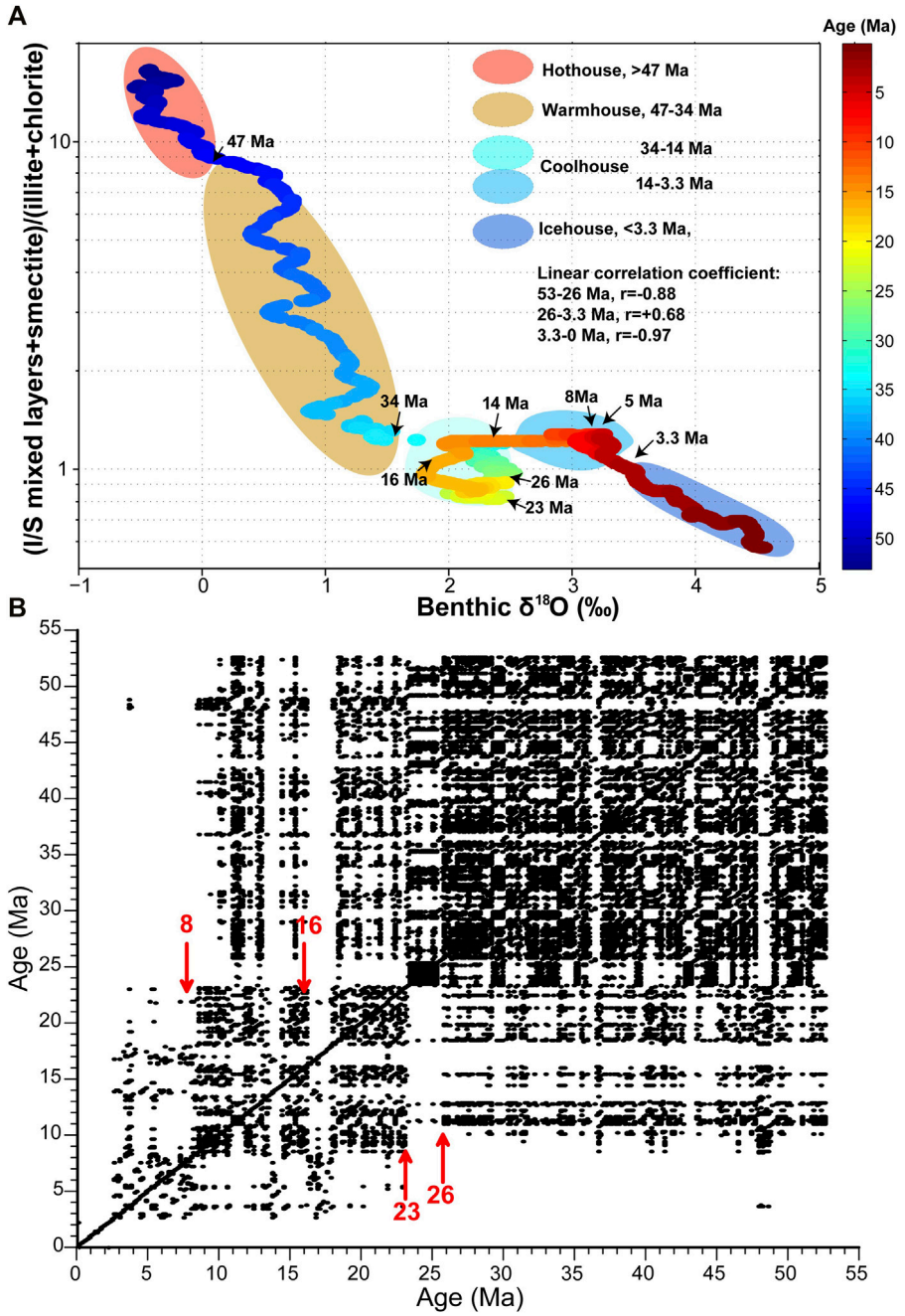

FIGURE 3 | Transitions of silicate weathering intensity in the NE Tibetan Plateau **(A)** Biplot of the (I/S mixed layer + smectite)/(illite + chlorite) ratio (using the LOESS fitting data shown in **Figure 1**) versus benthic oxygen data (Westerhold et al., 2020), illustrating the relationship between the two signals since 53 Ma. The four climate states (Hothouse, Warmhouse, Coolhouse, and Icehouse) are from Westerhold et al. (2020). Note the interruption of the pronounced negative correlation between the two signals during the Coolhouse state after ~26–23 Ma **(B)** Recurrence plots of (I/S mixed layer + smectite)/(illite + chlorite) ratio, showing patterns of climate change and major system transitions. The dark shading indicates intervals with similar weathering dynamics, and the unshaded areas indicate intervals with no common dynamics. The three major transitions are indicated by red arrows.

The three transition periods, marked by the onset of an enhanced SWI, coincide with stages of an intensified EASM. The first transition at ~26–23 Ma corresponds to the well documented reorganization of the Asian climate system, with the migration of the EASM into subtropical China, at the Oligocene-Miocene boundary (Sun and Wang, 2005; Guo et al., 2008). This Asian climate reorganization is assumed to be caused by Tibetan Plateau uplift and the retreat of the

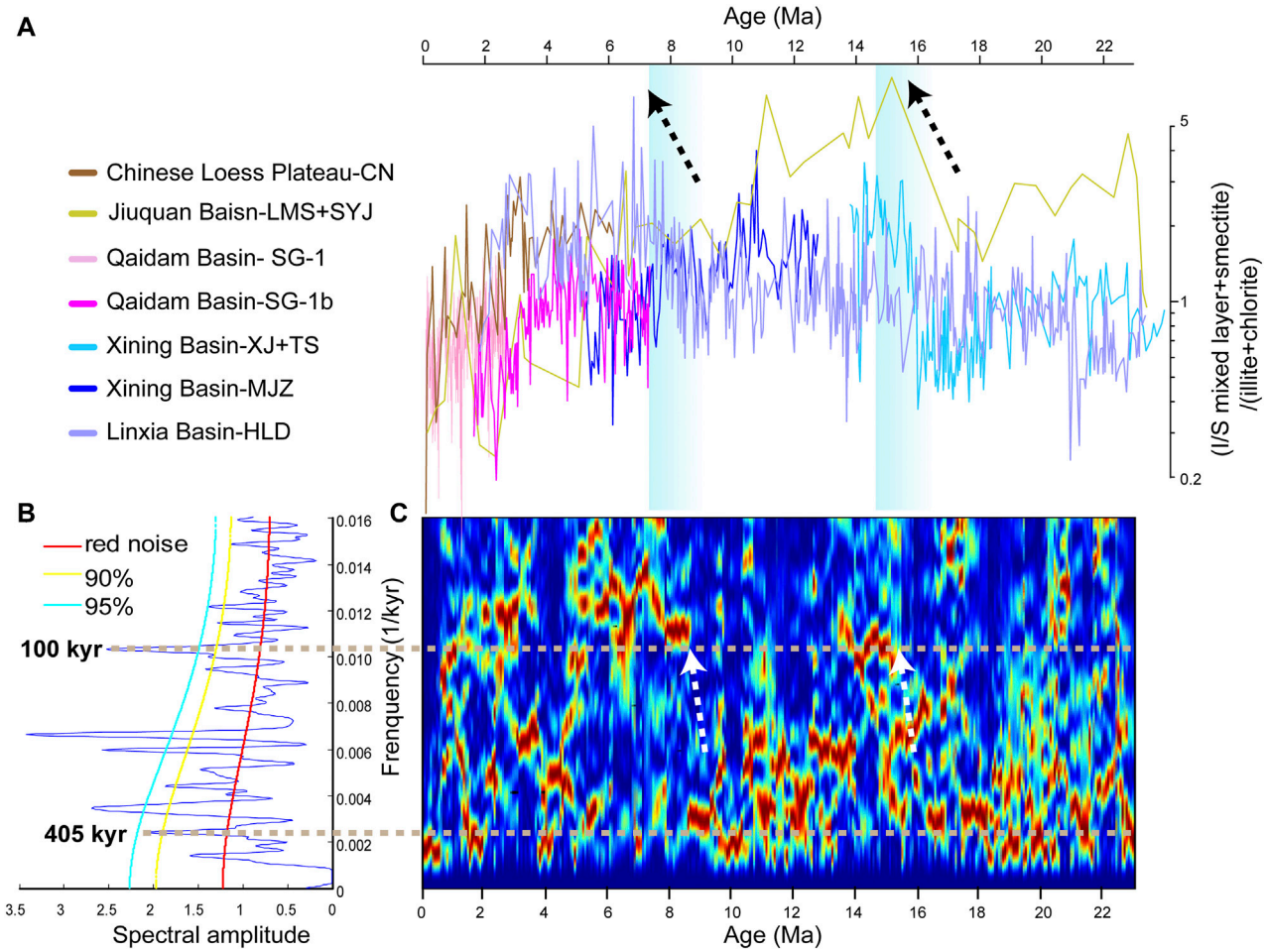

FIGURE 4 | Orbital-scale variability of silicate weathering intensity since 23 Ma **(A)** Compiled (I/S mixed layer + smectite)/(illite + chlorite) ratio since 23 Ma **(B)** 2π-Multi-taper method (MTM) power spectrum of the (I/S mixed layer + smectite)/(illite + chlorite) ratio, and **(C)** evolutive Fast Fourier transform spectrum used a 400-kyr sliding window, with a robust red-noise model at the 95% confidence level. The bold white arrows in **(C)** show an intensified eccentricity 100-kyr cycle at ~16 Ma and ~8 Ma.

Para-Tethys sea (e.g., Ramstein et al., 1997; Fluteau et al., 1999; Zhang et al., 2007a, Zhang et al., 2007b), during which the retreat of the Para-Tethys sea could be regarded as a far-field effect of the India-Asia collision. Such tectonics-driven northward migration of the intensified EASM was considered to have promoted increased rainfall in subtropical China and the NE Tibetan Plateau, thus facilitating silicate weathering (Yang et al., 2021d). The Middle Miocene was another period of EASM strengthening, which may have been caused by Tibetan Plateau uplift (Liu and Yin, 2002; Zhang R. et al., 2015) or global warming (Westerhold et al., 2020). Both factors could have resulted in a generally humid climate in the NE Tibetan Plateau (Miao et al., 2011; Hui et al., 2018), and hence a strengthened silicate weathering intensity (**Figure 2A**, Song Y. et al., 2018). However, we cannot precisely distinguish the respective contributions of regional uplift and the global climate to driving the transition at ~16 Ma. Nevertheless, the inconsistent correlation between the SWI record and global climate change (**Figure 3A**), and the abundant evidence for Middle Miocene uplift of the Tibetan Plateau (e.g., Lu et al., 2016; Yu et al., 2019), imply the pivotal role of tectonic uplift. The interval of ~9–8 Ma corresponds to an important intensification of the EASM, which is considered to have been induced by the coeval uplift of the Himalaya-Tibetan Plateau (Zheng et al., 2004; Sun et al., 2015; Yang et al., 2021b). Therefore, we conclude that the three identified transition periods in the SWI record for the NE Tibetan Plateau were linked to the regional intensification of silicate weathering driven by increased monsoon rainfall after ~26–23 Ma, which contrasts with the weaker silicate weathering before ~26–23 Ma that resulted from global cooling.

Spectral analysis of the SWI record provides additional information on the silicate weathering history and the underlying driving mechanism. The SWI has an average resolution of 63 kyr before 23 Ma, and 25 kyr thereafter (**Supplementary Figure S3**). The resolution before 23 Ma is inadequate for capturing orbital variability, but the subsequent resolution is sufficient to assess orbital variability within the eccentricity band (100 and 405 kyr). Therefore, spectral analysis was performed on the post-23 Ma interval of the SWI record.

The results show strong power in the 405-kyr, 100-kyr, 150–200kyr bands after 23 Ma (**Figure 4B**), accompanied by two major periodicity transitions characterized by prominent enhancements of the ~100-kyr band at ~16 Ma and ~8 Ma (**Figure 4C**). These two transitions on orbital cycles coincide with an enhanced monsoon and hence SWI, as mentioned above (**Figure 4A**). This coincidence between the emergence or intensification of 100-kyr cycle in the SWI records in the NE Tibetan Plateau and an enhanced EASM, was also reported in previous studies from the NE Tibetan Plateau. For example, Nie et al. (2017) and Wang et al. (2019, 2021) pointed out that lake expansion cycles in the Lanzhou, Guide and Qaidam Basins in the Early and Late Miocene were dominated by ~100 kyr eccentricity variance. And they assumed this cycle as derived from the EASM modulated by Antarctic ice sheets at the orbital scale (Nie et al., 2017; Wang et al., 2019; Wang et al. 2021). The variations of the Antarctic ice sheets are primarily presented as its intermittent development since ~42 Ma followed by a permanent development since the Eocene-Oligocene transition at 34 Ma, and a subsequent enhancement after the Mid-Miocene Climatic Optimum at 14 Ma (Tripati et al., 2005; Westerhold et al., 2020). The onset of an enhanced EASM at ~16 and ~8 Ma is suggested as a result of the Tibetan Plateau uplift at a tectonic scale. Therefore, the consistency between an enhanced EASM and the intensification of 100-kyr variance in our SWI record at ~16 and 8 Ma, implies a possible joint effect from both the Antarctic ice sheets and the tectonic uplift of the Tibetan Plateau and their interaction on modulating the evolution of the EASM and regional silicate weathering on an orbital scale. This joint effect or interaction can be performed as follows: the tectonic uplift, as the first driver, initially led to an enhanced erosion and promoted EASM intensity, both of which accelerate the silicate weathering and atmospheric CO_2 drawdown. This perturbation on the global carbon cycle subsequently facilitate the development of the Antarctic ice sheets (e.g., Tripati et al., 2005), which would exert influences on the monsoon system and affect the silicate weathering intensity of the studied regions. Additionally, in a Neogene world with low atmospheric CO_2 levels, a subtle change in pCO_2 within the error of the proxy estimates may be important in triggering ice-volume changes (Zachos et al., 2001). The strength of the silicate weathering feedback would also increase in a tectonically active world, implying that feedback in response to an initial increase in the weathering flux, which removes CO_2, could occur in a much more transient way (Caves et al., 2016; Caves Rugenstein et al., 2019). All the evidence jointly suggests that the orbital scale variations in the SWI in the NE Tibetan Plateau could stem from the interactions between tectonic uplift and the Antarctic ice sheets.

However, we need to stress that the inconsistent sampling resolution retrieved from different sections would limit a deeper discussion on the obtained 100-kyr cycle and associated driving factors, and therefore call for more future studies based on high-resolution continuous records. Furthermore, the strong power in the 150–200 kyr band recorded in our data (**Figure 4B**), is likely an indication of obliquity modulation cycle (Hinnov, 2000; Laskar et al., 2004) as found in the late Cenozoic sediments from the Qaidam Basin (Zhang et al., 2021) and the aeolian deposits in the Chinese Loess Plateau (Zhang et al., 2022), or an indication of the ~173-kyr cycle that has been recently discovered in many sedimentary records globally (e.g., Boulila et al., 2018; Huang et al., 2021; Zhang et al., 2022). Such evidence suggests that the identified cycles centered at 150–200 kyr are potential stable cycles concealed in paleoenvironmental records in the central and east Asia, which requires more attention and further investigations.

CONCLUSION

We have constructed the first Cenozoic long-term silicate weathering history of the NE Tibetan Plateau, based on a compilation of the (I/S mixed layer + smectite)/(illite + chlorite) ratio from ten sections in the region. The silicate weathering intensity of the NE Tibetan Plateau is characterized by a long-term decrease during the Paleogene followed by a long-term enhancement during the Neogene. Three major transitions were detected in the regional silicate weathering history, at ~26–23 Ma, ~16 Ma, and ~8 Ma. The ~26–23 Ma, ~16 Ma and ~8 Ma transitions identified in stacked SWI record accompanied by the intensification of 100-kyr eccentricity cycle at ~16 Ma and ~8 Ma in SWI record, are coincide with enhanced EASM at these intervals. We suggest that global climate state is the dominant factor modulating the variations of silicate weathering of the NE Tibetan Plateau during the Paleogene, while its Neogene variations and the three identified critical transitions are more related to the regional monsoon rainfall. The ~16 Ma and ~8 Ma transitions coincide with an intensified 100-kyr eccentricity cycle, which may result that resulted from a joint effect of both the Antarctic ice sheets and the Tibetan Plateau uplift and their possible interaction on the EASM and regional silicate weathering on timescales of 10^5–10^6 years. Such interaction might stem from an increased feedback strength of silicate weathering and other environmental variables (e.g., ice volume) under a tectonically active Neogene world with a low CO_2 level.

DATA AVAILABILITY STATEMENT

The original contributions presented in the study are included in the article/**Supplementary Material**, further inquiries can be directed to the corresponding authors.

AUTHOR CONTRIBUTIONS

YY, XF designed the research. YY and CY performed the clay mineral analyses and collected the data. YY, WH and AG interpreted the data, and YY and WH prepared the manuscript with contributions from all co-authors.

FUNDING

This work was co-supported by the Basic Science Center for Tibetan Plateau Earth System (CTPES, 41988101-01), the Second Tibetan Plateau Scientific Expedition and Research (STEP) program (Grant No. 2019QZKK0707), the National Natural Science Foundation of China (Grant Nos. 41771236, 41872098, and 42071111), the Strategic Priority Research Program of the Chinese Academy of Sciences (Grant No. XDA20070201). YY is supported by the Youth Innovation Promotion Association (2018095) of the Chinese Academy of Sciences.

ACKNOWLEDGMENTS

We thank Jan Bloemendal for polishing language.

SUPPLEMENTARY MATERIAL

The Supplementary Material for this article can be found online at: https://www.frontiersin.org/articles/10.3389/feart.2022.824404/full#supplementary-material

REFERENCES

Bao, J., Song, C., Yang, Y., Fang, X., Meng, Q., Feng, Y., et al. (2019). Reduced Chemical Weathering Intensity in the Qaidam Basin (NE Tibetan Plateau) during the Late Cenozoic. *J. Asian Earth Sci.* 170, 155–165. doi:10.1016/j.jseaes.2018.10.018

Bao, J., Wang, Y., Song, C., Feng, Y., Hu, C., Zhong, S., et al. (2017). Cenozoic Sediment Flux in the Qaidam Basin, Northern Tibetan Plateau, and Implications with Regional Tectonics and Climate. *Glob. Planet. Change* 155, 56–69. doi:10.1016/j.gloplacha.2017.03.006

Blum, J. D., Gazis, C. A., Jacobson, A. D., and Page Chamberlain, C. (1998). Carbonate versus Silicate Weathering in the Raikhot Watershed within the High Himalayan Crystalline Series. *Geol* 26 (5), 411–414. doi:10.1130/0091-7613(1998)026<0411:cvswit>2.3.co;2

Boulila, S., Vahlenkamp, M., De Vleeschouwer, D., Laskar, J., Yamamoto, Y., Pälike, H., et al. (2018). Towards a Robust and Consistent Middle Eocene Astronomical Timescale. *Earth Planet. Sci. Lett.* 486, 94–107. doi:10.1016/j.epsl.2018.01.003

Bush, M. A., Saylor, J. E., Horton, B. K., and Nie, J. (2016). Growth of the Qaidam Basin during Cenozoic Exhumation in the Northern Tibetan Plateau: Inferences from Depositional Patterns and Multiproxy Detrital Provenance Signatures. *Lithosphere* 8 (1), 58–82. doi:10.1130/L449.1

Caves, J. K., Jost, A. B., Lau, K. V., and Maher, K. (2016). Cenozoic Carbon Cycle Imbalances and a Variable Weathering Feedback. *Earth Planet. Sci. Lett.* 450, 152–163. doi:10.1016/j.epsl.2016.06.035

Caves Rugenstein, J. K., Ibarra, D. E., and von Blanckenburg, F. (2019). Neogene Cooling Driven by Land Surface Reactivity rather Than Increased Weathering Fluxes. *Nature* 571 (7763), 99–102. doi:10.1038/s41586-019-1332-y

Chamley, H. (1989). *Clay Sedimentology*. Berlin: Springer-Verlag. doi:10.1007/978-3-642-85916-8

Clark, M. K., Farley, K. A., Zheng, D., Wang, Z., and Duvall, A. R. (2010). Early Cenozoic Faulting of the Northern Tibetan Plateau Margin from Apatite (U-Th)/He Ages. *Earth Planet. Sci. Lett.* 296 (1-2), 78–88. doi:10.1016/j.epsl.2010.04.051

Chen, Z., and Li, G. (2013). Evolving sources of eolian detritus on the Chinese Loess Plateau since early Miocene: Tectonic and climatic controls. *Earth Planet. Sci. Lett.* 371, 220–225. doi:10.1016/j.epsl.2013.03.044

Cleveland, W. S., and Devlin, S. J. (1988). Locally Weighted Regression: An Approach to Regression Analysis by Local Fitting. *J. Am. Stat. Assoc.* 83 (403), 596–610. doi:10.1080/01621459.1988.10478639

Dai, S., Fang, X., Dupont-Nivet, G., Song, C., Gao, J., Krijgsman, W., et al. (2006). Magnetostratigraphy of Cenozoic Sediments from the Xining Basin: Tectonic Implications for the Northeastern Tibetan Plateau. *J. Geophys. Res.* 111, a–n. doi:10.1029/2005JB004187

Fang, X., Zhao, Z., Li, J., Yan, M., Pan, B., Song, C., et al. (2005). Magnetostratigraphy of the Late Cenozoic Laojunmiao Anticline in the Northern Qilian Mountains and its Implications for the Northern Tibetan Plateau Uplift. *Sci. China Ser. D* 48 (7), 1040–1051. doi:10.1360/03yd0188

Fang, X., Li, M., Wang, Z., Wang, J., Li, J., Liu, X., et al. (2016a). Oscillation of mineral Compositions in Core SG-1b, Western Qaidam Basin, NE Tibetan Plateau. *Sci. Rep.* 6 (1), 1–7. doi:10.1038/srep32848

Fang, X., Wang, J., Zhang, W., Zan, J., Song, C., Yan, M., et al. (2016b). Tectonosedimentary Evolution Model of an Intracontinental Flexural (Foreland) basin for Paleoclimatic Research. *Glob. Planet. Change* 145, 78–97. doi:10.1016/j.gloplacha.2016.08.015

Fang, X., Fang, Y., Zan, J., Zhang, W., Song, C., Appel, E., et al. (2019a). Cenozoic Magnetostratigraphy of the Xining Basin, NE Tibetan Plateau, and its Constraints on Paleontological, Sedimentological and Tectonomorphological Evolution. *Earth-Science Rev.* 190, 460–485. doi:10.1016/j.earscirev.2019.01.021

Fang, X., Galy, A., Yang, Y., Zhang, W., Ye, C., and Song, C. (2019b). Paleogene Global Cooling-Induced Temperature Feedback on Chemical Weathering, as Recorded in the Northern Tibetan Plateau. *Geology* 47 (10), 992–996. doi:10.1130/G46422.1

Fluteau, F., Ramstein, G., and Besse, J. (1999). Simulating the Evolution of the Asian and African Monsoons during the Past 30 Myr Using an Atmospheric General Circulation Model. *J. Geophys. Res.* 104, 11995–12018. doi:10.1029/1999jd900048

Foster, G. L., Royer, D. L., and Lunt, D. J. (2017). Future Climate Forcing Potentially without Precedent in the Last 420 Million Years. *Nat. Commun.* 8 (1), 1–8. doi:10.1038/ncomms14845

France-Lanord, C., and Derry, L. A. (1997). Organic Carbon Burial Forcing of the Carbon Cycle from Himalayan Erosion. *Nature* 390 (6655), 65–67. doi:10.1038/36324

Guo, Y., Yang, S., Su, N., Li, C., Yin, P., and Wang, Z. (2018). Revisiting the Effects of Hydrodynamic Sorting and Sedimentary Recycling on Chemical Weathering Indices. *Geochimica et Cosmochimica Acta* 227, 48–63. doi:10.1016/j.gca.2018.02.015

Guo, Z. T., Sun, B., Zhang, Z. S., Peng, S. Z., Xiao, G. Q., Ge, J. Y., et al. (2008). A Major Reorganization of Asian Climate by the Early Miocene. *Clim. Past* 4 (3), 153–174. doi:10.5194/cp-4-153-2008

Guo, Z., Wilson, M., Dingwell, D. B., and Liu, J. (2021). India-asia Collision as a Driver of Atmospheric CO2 in the Cenozoic. *Nat. Commun.* 12 (1), 1–15. doi:10.1038/s41467-021-23772-y

He, Z., Guo, Z., Yang, F., Sayem, A. S. M., Wu, H., Zhang, C., et al. (2019). Provenance of Cenozoic Sediments in the Xining Basin Revealed by Nd and Pb Isotopic Evidence: Implications for Tectonic Uplift of the NE Tibetan Plateau. *Geochem. Geophys. Geosyst.* 20 (10), 4531–4544. doi:10.1029/2019GC008556

Higgins, J. A., and Schrag, D. P. (2015). The Mg Isotopic Composition of Cenozoic Seawater - Evidence for a Link between Mg-Clays, Seawater Mg/Ca, and Climate. *Earth Planet. Sci. Lett.* 416, 73–81. doi:10.1016/j.epsl.2015.01.003

Hinnov, L. A. (2000). New Perspectives on Orbitally Forced Stratigraphy. *Annu. Rev. Earth Planet. Sci.* 28, 419–475. doi:10.1146/annurev.earth.28.1.419

Huang, H., Gao, Y., Ma, C., Jones, M. M., Zeeden, C., Ibarra, D. E., et al. (2021). Organic Carbon Burial Is Paced by a ~173-ka Obliquity Cycle in the Middle to High Latitudes. *Sci. Adv.* 7, eabf9489. doi:10.1126/sciadv.abf9489

Hui, Z., Zhang, J., Ma, Z., Li, X., Peng, T., Li, J., et al. (2018). Global Warming and Rainfall: Lessons from an Analysis of Mid-miocene Climate Data. *Palaeogeogr. Palaeoclimatol. Palaeoecol.* 512, 106–117. doi:10.1016/j.palaeo.2018.10.025

Kump, L. R., and Arthur, M. A. (1997). "Global Chemical Erosion during the Cenozoic: Weatherability Balances the Budgets," in *Tectonic Uplift and Climate Change* (Springer US), 399–426. doi:10.1007/978-1-4615-5935-1_18

Laskar, J., Correia, A. C. M., Gastineau, M., Joutel, F., Levrard, B., and Robutel, P. (2004). Long Term Evolution and Chaotic Diffusion of the Insolation Quantities of mars. *Icarus* 170, 343–364. doi:10.1016/j.icarus.2004.04.005

Lee, T. Y., and Lawver, L. A. (1995). Cenozoic Plate Reconstruction of Southeast Asia. *Tectonophysics* 251 (1-4), 85–138. doi:10.1016/0040-1951(95)00023-2

Lenard, S. J. P., Lavé, J., France-Lanord, C., Aumaître, G., Bourlès, D. L., and Keddadouche, K. (2020). Steady Erosion Rates in the Himalayas through Late

Cenozoic Climatic Changes. *Nat. Geosci.* 13 (6), 448–452. doi:10.1038/s41561-020-0585-2

Li, J. X., Yue, L. P., Roberts, A. P., Hirt, A. M., Pan, F., Guo, L., et al. (2018). Global Cooling and Enhanced Eocene Asian Mid-latitude interior Aridity. *Nat. Commun.* 9 (1), 3026. doi:10.1038/s41467-018-05415-x

Li, M., Sun, S., Fang, X., Wang, C., Wang, Z., and Wang, H. (2018). Clay Minerals and Isotopes of Pleistocene Lacustrine Sediments from the Western Qaidam Basin, NE Tibetan Plateau. *Appl. Clay Sci.* 162, 382–390. doi:10.1016/j.clay.2018.06.033

Licht, A., Dupont-Nivet, G., Pullen, A., Kapp, P., Abels, H. A., Lai, Z., et al. (2016). Resilience of the Asian Atmospheric Circulation Shown by Paleogene Dust Provenance. *Nat. Commun.* 7 (1), 1–6. doi:10.1038/ncomms12390

Liu, X., and Yin, Z. Y. (2002). Sensitivity of East Asian Monsoon Climate to the Uplift of the Tibetan Plateau. *Paleogeogr. Paleoclimatol. Paleoecol.* 183 (3-4), 223–245. doi:10.1016/S0031-0182(01)00488-6

Liu, Y., Song, C., Meng, Q., He, P., Yang, R., Huang, R., et al. (2020). Paleoclimate Change since the Miocene Inferred from clay-mineral Records of the Jiuquan Basin, NW China. *Palaeogeogr. Palaeoclimatol. Palaeoecol.* 550, 109730. doi:10.1016/j.palaeo.2020.109730

Liu, Z., Hong, H., Wang, C., Han, W., Yin, K., Ji, K., et al. (2019). Oligocene-Miocene (28-13 Ma) Climato-Tectonic Evolution of the Northeastern Qinghai-Tibetan Plateau Evidenced by Mineralogical and Geochemical Records of the Xunhua Basin. *Palaeogeogr. Palaeoclimatol. Palaeoecol.* 514, 98–108. doi:10.1016/j.palaeo.2018.10.009

Lu, H., Fu, B., Shi, P., Ma, Y., and Li, H. (2016). Constraints on the Uplift Mechanism of Northern Tibet. *Earth Planet. Sci. Lett.* 453, 108–118. doi:10.1016/j.epsl.2016.08.010

Maher, K., and Chamberlain, C. P. (2014). Hydrologic Regulation of Chemical Weathering and the Geologic Carbon Cycle. *Science* 343 (6178), 1502–1504. doi:10.1126/science.1250770

Marwan, N., Carmenromano, M., Thiel, M., and Kurths, J. (2007). Recurrence Plots for the Analysis of Complex Systems. *Phys. Rep.* 438 (5-6), 237–329. doi:10.1016/j.physrep.2006.11.001

McCauley, S. E., and DePaolo, D. J. (1997). "The Marine 87Sr/86Sr and δ18O Records, Himalayan Alkalinity Fluxes, and Cenozoic Climate Models," in *Tectonic Uplift and Climate Change* (Boston, MA: Springer), 427–467. doi:10.1007/978-1-4615-5935-1_19

McLennan, S. M., Hemming, S., McDaniel, D. K., and Hanson, G. N. (1993). Geochemical Approaches to Sedimentation, Provenance, and Tectonics. *Process. Controlling Compost. Clastic Sediments,Geological Soc. America Spec. Pap.*, 21–40. doi:10.1130/SPE284-p21

Métivier, F., Gaudemer, Y., Tapponnier, P., and Klein, M. (1999). Mass Accumulation Rates in Asia during the Cenozoic. *Geophys. J. Int.* 137 (2), 280–318. doi:10.1046/j.1365-246X.1999.00802.x

Miao, Y., Fang, X., Herrmann, M., Wu, F., Zhang, Y., and Liu, D. (2011). Miocene Pollen Record of KC-1 Core in the Qaidam Basin, NE Tibetan Plateau and Implications for Evolution of the East Asian Monsoon. *Palaeogeogr. Palaeoclimatol. Palaeoecol.* 299 (1-2), 30–38. doi:10.1016/j.palaeo.2010.10.026

Misra, S., and Froelich, P. N. (2012). Lithium Isotope History of Cenozoic Seawater: Changes in Silicate Weathering and Reverse Weathering. *Science* 335 (6070), 818–823. doi:10.1126/science.1214697

Molnar, P., and Stock, J. M. (2009). Slowing of India's Convergence with Eurasia since 20 Ma and its Implications for Tibetan Mantle Dynamics. *Tectonics* 28 (3), a–n. doi:10.1029/2008TC002271

Nesbitt, H. W., and Young, G. M. (1982). Early Proterozoic Climates and Plate Motions Inferred from Major Element Chemistry of Lutites. *Nature* 299 (5885), 715–717. doi:10.1038/299715a0

Nie, J., Garzione, C., Su, Q., Liu, Q., Zhang, R., Heslop, D., et al. (2017). Dominant 100,000-year Precipitation Cyclicity in a Late Miocene lake from Northeast Tibet. *Sci. Adv.* 3 (3), e1600762. doi:10.1126/sciadv.1600762

Nie, J., Stevens, T., Rittner, M., Stockli, D., Garzanti, E., Limonta, M., et al. (2015). Loess Plateau Storage of Northeastern Tibetan Plateau-Derived Yellow River Sediment. *Nat. Commun.* 6, 8511. doi:10.1038/ncomms9511

Paytan, A., Griffith, E. M., Eisenhauer, A., Hain, M. P., Wallmann, K., and Ridgwell, A. (2021). A 35-Million-Year Record of Seawater Stable Sr Isotopes Reveals a Fluctuating Global Carbon Cycle. *Science* 371 (6536), 1346–1350. doi:10.1126/science.aaz9266

Peucker-Ehrenbrink, B., Ravizza, G., and Hofmann, A. W. (1995). The marine $^{187}Os/^{186}Os$ Record of the Past 80-million Years. *Earth Planet. Sci. Lett.* 130 (1-4). doi:10.1016/0012-821X(95)00003-U

Pullen, A., Kapp, P., McCallister, A. T., Chang, H., Gehrels, G. E., Garzione, G. N., et al. (2021). Qaidam Basin and northern Tibetan Plateau as dust sources for the Chinese Loess Plateau and paleoclimatic implications. *Geology* 39, 1031–1034. doi:10.1130/G32296.1

Ramstein, G., Fluteau, F., Besse, J., and Joussaume, S. (1997). Effect of Orogeny, Plate Motion and Land-Sea Distribution on Eurasian Climate Change over the Past 30 Million Years. *Nature* 386, 788–795. doi:10.1038/386788a0

Raymo, M. E., and Ruddiman, W. F. (1992). Tectonic Forcing of Late Cenozoic Climate. *Nature* 359 (6391), 117–122. doi:10.1038/359117a0

Ren, X., Nie, J., Saylor, J. E., Wang, X., Liu, F., and Horton, B. K. (2020). Temperature Control on Silicate Weathering Intensity and Evolution of the Neogene East Asian Summer Monsoon. *Geophys. Res. Lett.* 47 (15), e2020GL088808. doi:10.1029/2020GL088808

Richter, F. M., Rowley, D. B., and DePaolo, D. J. (1992). Sr Isotope Evolution of Seawater: the Role of Tectonics. *Earth Planet. Sci. Lett.* 109 (1-2), 11–23. doi:10.1016/0012-821X(92)90070-C

Sayem, A. S. M., Guo, Z., Wu, H., Zhang, C., Yang, F., Xiao, G., et al. (2018). Sedimentary and Geochemical Evidence of Eocene Climate Change in the Xining Basin, Northeastern Tibetan Plateau. *Sci. China Earth Sci.* 61 (9), 1292–1305. doi:10.1007/s11430-018-9231-9

Song, B., Zhang, K., Lu, J., Wang, C., and Xu, Y. (2013). The Middle Eocene to Early Miocene Integrated Sedimentary Record in the Qaidam Basin and its Implications for Paleoclimate and Early Tibetan Plateau Uplift. *Can. J. Earth Sci.* 50 (2), 183–196. doi:10.1139/cjes-2012-0048

Song, B., Zhang, K., Zhang, L., Ji, J., Hong, H., Wei, Y., et al. (2018). Qaidam Basin Paleosols Reflect Climate and Weathering Intensity on the Northeastern Tibetan Plateau during the Early Eocene Climatic Optimum. *Palaeogeogr. Palaeoclimatol. Palaeoecol.* 512, 6–22. doi:10.1016/j.palaeo.2018.03.027

Song, C. (2006). *The Cenozoic Sedimentary Evolution and Plateau Tectonic Uplift Process of the Northern Margin of the Qinghai-Tibet Plateau [Doctor's Thesis]* (Lanzhou: Lanzhou university).

Song, Y., Fang, X., Li, J., An, Z., and Miao, X. (2001). The Late Cenozoic Uplift of the Liupan Shan, China. *Sci. China Ser. D-earth Sci.* 44, 176–184. doi:10.1007/BF02911985

Song, Y., Wang, Q., An, Z., Qiang, X., Dong, J., Chang, H., et al. (2018). Mid-Miocene Climatic Optimum: Clay mineral Evidence from the Red clay Succession, Longzhong Basin, Northern China. *Palaeogeogr. Palaeoclimatol. Palaeoecol.* 512, 46–55. doi:10.1016/j.palaeo.2017.10.001

Song, Z., Wan, S., Colin, C., Yu, Z., Révillon, S., Jin, H., et al. (2021). Paleoenvironmental Evolution of South Asia and its Link to Himalayan Uplift and Climatic Change since the Late Eocene. *Glob. Planet. Change* 200 (5), 103459. doi:10.1016/j.gloplacha.2021.103459

Sun, X., and Wang, P. (2005). How Old Is the Asian Monsoon System?-Palaeobotanical Records from China. *Palaeogeogr. Palaeoclimatol. Palaeoecol.* 222 (3-4), 181–222. doi:10.1016/j.palaeo.2005.03.005

Sun, Y., Liu, J., Liang, Y., Ji, J., Liu, W., Aitchison, J. C., et al. (2020). Cenozoic Moisture Fluctuations on the Northeastern Tibetan Plateau and Association with Global Climatic Conditions. *J. Asian Earth Sci.* 200, 104490. doi:10.1016/j.jseaes.2020.104490

Sun, Y., Ma, L., Bloemendal, J., Clemens, S., Qiang, X., and An, Z. (2015). Miocene Climate Change on the Chinese Loess Plateau: Possible Links to the Growth of the Northern Tibetan Plateau and Global Cooling. *Geochem. Geophys. Geosyst.* 16 (7), 2097–2108. doi:10.1002/2015GC005750

Tapponnier, P., Zhiqin, X., Roger, F., Meyer, B., Arnaud, N., Wittlinger, G., et al. (2001). Oblique Stepwise Rise and Growth of the Tibet Plateau. *Science* 294 (5547), 1671–1677. doi:10.1126/science.105978

Tripati, A., Backman, J., Elderfield, H., and Ferretti, P. (2005). Eocene Bipolar Glaciation Associated with Global Carbon Cycle Changes. *Nature* 436 (7049), 341–346. doi:10.1038/nature03874

van Hinsbergen, D. J. J., Steinberger, B., Doubrovine, P. V., and Gassmöller, R. (2011). Acceleration and Deceleration of India-Asia Convergence since the Cretaceous: Roles of Mantle Plumes and continental Collision. *J. Geophys. Res.* 116, B06101. doi:10.1029/2010JB008051

Walker, J. C. G., Hays, P. B., and Kasting, J. F. (1981). A Negative Feedback Mechanism for the Long-Term Stabilization of Earth's Surface Temperature. *J. Geophys. Res.* 86 (C10), 9776–9782. doi:10.1029/JC086iC10p09776

Wang, F., Shi, W., Zhang, W., Wu, L., Yang, L., Wang, Y., et al. (2017). Differential Growth of the Northern Tibetan Margin: Evidence for Oblique Stepwise Rise of the Tibetan Plateau. *Sci. Rep.* 7 (1), 1–9. doi:10.1038/srep41164

Wang, Z., Huang, C., Licht, A., Zhang, R., and Kemp, D. B. (2019). Middle to Late Miocene Eccentricity Forcing on lake Expansion in NE Tibet. *Geophys. Res. Lett.* 46 (12), 6926–6935. doi:10.1029/2019GL082283

Wang, Z., Zhang, Z., Huang, C., Shen, J., Sui, Y., and Qian, Z. (2021). Astronomical Forcing of lake Evolution in the Lanzhou Basin during Early Miocene Period. *Earth Planet. Sci. Lett.* 554, 116648. doi:10.1016/j.epsl.2020.116648

Weaver, C. E. (1989). *Clays, Muds, and Shales*. Amsterdam: Elsevier, Developments in Sedimentology 44, 819 p. doi:10.1016/0037-0738(91)90107-O

Weaver, C. E. (1984). *Shale-slate Metamorphism in Southern Appalachians*. Amsterdam: Elsevier. doi:10.1016/B978-0-444-42264-4.50011-6

Westerhold, T., Marwan, N., Drury, A. J., Liebrand, D., Agnini, C., Anagnostou, E., et al. (2020). An Astronomically Dated Record of Earth's Climate and its Predictability over the Last 66 Million Years. *Science* 369 (6509), 1383–1387. doi:10.1126/science.aba6853

Willenbring, J. K., and Von Blanckenburg, F. (2010). Long-term Stability of Global Erosion Rates and Weathering during Late-Cenozoic Cooling. *Nature* 465 (7295), 211–214. doi:10.1038/nature09044

Yang, R., Fang, X., Meng, Q., Zan, J., Zhang, W., Deng, T., et al. (2017). Paleomagnetic constraints on the middle Miocene-early Pliocene stratigraphy in the Xining Basin, NE Tibetan Plateau, and the geologic implications. *Geochem. Geophys. Geosyst.* 18 (11), 3741–3757. doi:10.1002/2017GC006945

Yang, R., Yang, Y., Fang, X., Ruan, X., Galy, A., Ye, C., et al. (2019). Late Miocene Intensified Tectonic Uplift and Climatic Aridification on the Northeastern Tibetan Plateau: Evidence from clay Mineralogical and Geochemical Records in the Xining Basin. *Geochem. Geophys. Geosyst.* 20 (2), 829–851. doi:10.1029/2018GC007917

Yang, Y., Galy, A., Fang, X., Yang, R., Zhang, W., Song, B., et al. (2021a). Neodymium Isotopic Constraints on Cenozoic Asian Dust Provenance Changes Linked to the Exhumation History of the Northern Tibetan Plateau and the Central Asian Orogenic Belt. *Geochimica et Cosmochimica Acta* 296, 38–55. doi:10.1016/j.gca.2020.12.026

Yang, Y., Ye, C., Galy, A., Fang, X., Xue, Y., Liu, Y., et al. (2021b). Monsoon-Enhanced Silicate Weathering as a New Atmospheric CO 2 Consumption Mechanism Contributing to Fast Late Miocene Global Cooling. *Paleoceanogr Paleoclimatol* 36 (1), e2020PA004008. doi:10.1029/2020PA004008

Yang, Y., Ye, C., Yang, R., and Fang, X. (2021c). Revisiting clay-sized mineral and Elemental Records of the Silicate Weathering History in the Northern Tibetan Plateau during the Late Cenozoic: The Role of Aeolian Dust. *Terra Nova* 33, 252–261. doi:10.1111/ter.12508

Yang, Y., Galy, A., Fang, X., France-Lanord, C., Wan, S., Yang, R., et al. (2021d). East Asian Monsoon Intensification Promoted Weathering of the Magnesium-Rich Southern China Upper Crust and its Global Significance. *Sci. China Earth Sci.* 64, 1155–1170. doi:10.1007/s11430-020-9781-3

Ye, C., Yang, Y., Fang, X., Hong, H., Wang, C., Yang, R., et al. (2018). Chlorite Chemical Composition Change in Response to the Eocene-Oligocene Climate Transition on the Northeastern Tibetan Plateau. *Palaeogeogr. Palaeoclimatol. Palaeoecol.* 512, 23–32. doi:10.1016/j.palaeo.2018.03.014

Ye, C., Yang, Y., Fang, X., Zan, J., Tan, M., and Yang, R. (2020). Chlorite Weathering Linked to Magnetic Enhancement in Red Clay on the Chinese Loess Plateau. *Palaeogeogr. Palaeoclimatol. Palaeoecol.* 538, 109446. doi:10.1016/j.palaeo.2019.109446

Yin, A., and Harrison, T. M. (2000). Geologic evolution of the Himalayan-Tibetan orogen. *Ann. Rev. Earth Planet. Sci.* 28 (1), 211–280. doi:10.1146/annurev.earth.28.1.211

Yu, J., Pang, J., Wang, Y., Zheng, D., Liu, C., Wang, W., et al. (2019). Mid-Miocene Uplift of the Northern Qilian Shan as a Result of the Northward Growth of the Northern Tibetan Plateau. *Geosphere* 15 (2), 423–432. doi:10.1130/GES01520.1

Zachos, J., Pagani, M., Sloan, L., Thomas, E., and Billups, K. (2001). Trends, Rhythms, and Aberrations in Global Climate 65 Ma to Present. *Science* 292 (5517), 686–693. doi:10.1126/science.1059412

Zan, J., Fang, X., Yan, M., Zhang, W., and Lu, Y. (2015). Lithologic and Rock Magnetic Evidence for the Mid-miocene Climatic Optimum Recorded in the Sedimentary Archive of the Xining Basin, NE Tibetan Plateau. *Palaeogeogr. Palaeoclimatol. Palaeoecol.* 431, 6–14. doi:10.1016/j.palaeo.2015.04.024

Zhang, C., and Guo, Z. (2014). Clay mineral Changes across the Eocene-Oligocene Transition in the Sedimentary Sequence at Xining Occurred Prior to Global Cooling. *Palaeogeogr. Palaeoclimatol. Palaeoecol.* 411, 18–29. doi:10.1016/j.palaeo.2014.06.031

Zhang, C., Xiao, G., Guo, Z., Wu, H., and Hao, Q. (2015). Evidence of Late Early Miocene Aridification Intensification in the Xining Basin Caused by the Northeastern Tibetan Plateau Uplift. *Glob. Planet. Change* 128, 31–46. doi:10.1016/j.gloplacha.2015.02.002

Zhang, R., Jiang, D., Zhang, Z., and Yu, E. (2015). The Impact of Regional Uplift of the Tibetan Plateau on the Asian Monsoon Climate. *Palaeogeogr. Palaeoclimatol. Palaeoecol.* 417, 137–150. doi:10.1016/j.palaeo.2014.10.030

Zhang, R., Li, X., Xu, Y., Li, J., Sun, L., Yue, L., et al. (2022). The 173-kyr Obliquity Cycle Pacing the Asian Monsoon in the Eastern Chinese Loess Plateau from Late Miocene to Pliocene. *Geophys. Res. Lett.* 49, e2021GL097008. doi:10.1029/2021GL097008

Zhang, T., Han, W., Fang, X., Song, C., Wang, Y., Tian, Q., et al. (2021). Tectonic Forcing of Environmental Transition in Central Asia at ~11-9 Ma. *Gondwana Res.* 89, 19–30. doi:10.1016/j.gr.2020.08.012

Zhang, W., Appel, E., Fang, X., Song, C., and Cirpka, O. (2012). Magnetostratigraphy of Deep Drilling Core SG-1 in the Western Qaidam Basin (NE Tibetan Plateau) and its Tectonic Implications. *Quat. Res.* 78 (1), 139–148. doi:10.1016/j.yqres.2012.03.011

Zhang, W., Appel, E., Fang, X., Song, C., Setzer, F., Herb, C., et al. (2014). Magnetostratigraphy of Drill-Core SG-1b in the Western Qaidam Basin (NE Tibetan Plateau) and Tectonic Implications. *Geophys. J. Int.* 197 (1), 90–118. doi:10.1093/gji/ggt439

Zhao, C., Wang, C., Hong, H., Algeo, T. J., Yin, K., Ji, K., et al. (2021). Origin of Dioctahedral Smectites in Lower Eocene Lulehe Formation Paleosols (Qaidam Basin, China). *Appl. Clay Sci.* 203, 106026. doi:10.1016/j.clay.2021.106026

Zheng, H., Powell, C. M., Rea, D. K., Wang, J., and Wang, P. (2004). Late Miocene and Mid-pliocene Enhancement of the East Asian Monsoon as Viewed from the Land and Sea. *Glob. Planet. Change* 41 (3-4), 147–155. doi:10.1016/j.gloplacha.2004.01.003

Zhang, Z., Wang, H., Guo, Z., and Jiang, D. (2007a). What Triggers the Transition of Palaeoenvironmental Patterns in China, the Tibetan Plateau Uplift or the Paratethys Sea Retreat?. *Palaeogeogr. Palaeoclimatol. Palaeoecol.* 245, 317–331. doi:10.1016/j.palaeo.2006.08.003

Zhang, Z., Huijun, W., Zhengtang, G., and Dabang, J. (2007b). Impacts of Tectonic Changes on the Reorganization of the Cenozoic Paleoclimatic Patterns in China. *Earth Planet. Sci. Lett.* 257, 622–634. doi:10.1016/j.epsl.2007.03.024

Zuza, A. V., Wu, C., Reith, R. C., Yin, A., Li, J., Zhang, J., et al. (2018). Tectonic Evolution of the Qilian Shan: An Early Paleozoic Orogen Reactivated in the Cenozoic. *Geol. Soc. Am. Bull.* 130 (5-6), 881–925. doi:10.1130/B31721.1

Conflict of Interest: The authors declare that the research was conducted in the absence of any commercial or financial relationships that could be construed as a potential conflict of interest.